

A Negative Cooperativity Mechanism of Human CYP2E1 Inferred from Molecular Dynamics Simulations and Free Energy Calculations

Jue Li,[†] Dong-Qing Wei,^{*,†} Jing-Fang Wang,^{*,‡,§} and Yi-Xue Li^{†,§,||}

[†]College of Life Science and Biotechnology and State Key Laboratory of Microbial Metabolism, Shanghai Jiao Tong University, Shanghai 200240, China

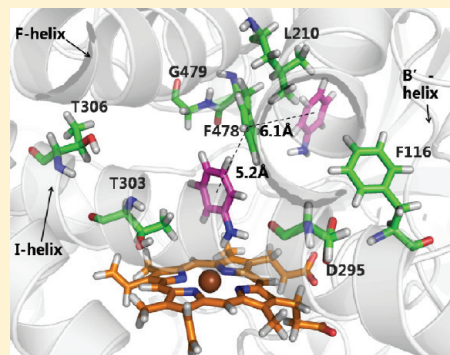
^{*}Key Laboratory of Systems Biomedicine (Ministry of Education), Shanghai Center for Systems Biomedicine, Shanghai Jiao Tong University, Shanghai 200240, China

[‡]Shanghai Center for Bioinformation Technology, 100 Qinzhou Road, Shanghai 200235, China

^{||}Key Laboratory of Systems Biology, Shanghai Institutes for Biological Sciences, Chinese Academy of Sciences, Shanghai 200031, China

S Supporting Information

ABSTRACT: Human cytochrome P450 2E1 (CYP2E1) participates in the metabolism of over 2% of all the oral drugs. A hallmark peculiar feature of this enzyme is that it exhibits a pronounced negative cooperativity in substrate binding. However the mechanism by which the negative cooperativity occurs is unclear. Here, we performed molecular dynamics simulations and free energy calculations on human CYP2E1 to examine the structural differences between the substrate-free and the enzymes with one and two aniline molecules bound. Our results indicate that although the effector substrate does not bind in the active site cavity, it still can directly interact with the active site residues of human CYP2E1. The interaction of the effector substrate with the active site leads to a reorientation of active site residues, which thereby weakens the interactions of the active substrate with this site. We also identify a conserved residue T303 that plays a crucial role in the negative cooperative binding on the short-range effects. This residue is a key factor in the positioning of substrates and in proton delivery to the active site. Additionally, a long-range effect of the effector substrate is identified in which F478 is proposed to play a key role. As located in the interface between the active and effector sites, this residue structurally links the active and effector sites and is found to play a significant role in affecting substrate access and ligand positioning within the active site. In the negative cooperative binding, this residue can decrease the interactions of the active substrate with the active site by $\pi-\pi$ stacking which then lowers the hydroxylation activity for the active substrate. These findings are in agreement with previous experimental observations and thus provide detailed atomistic insight into the poorly understood mechanism of the negative cooperativity in human CYP2E1.



INTRODUCTION

Cytochrome P450 2E1 (CYP2E1) is a heme-containing enzyme and belongs to the cytochrome P450 mixed-function oxidase system, which functions as a monooxygenase in many organisms to catalyze the oxidative metabolism of endogenous and exogenous compounds.^{1,2} Members of this family are medically significant, as this cytochrome family is believed to account for nearly 75% of the total drug metabolism. Polymorphic variations in these enzymes result in marked individual and population-wide differences in the tolerance to toxins and drugs.^{3–5} Human CYP2E1, a well studied member of this family, alone participates in the metabolism of more than 2% of all the oral drugs. This enzyme also recognizes many monocyclic and bicyclic compounds possessing minimal substitutions, such as *p*-nitrophenol, acetaminophen, and anilines. Thus, CYP2E1 is of particular interest to the pharmaceutical industry for its involvement in the metabolic processes of many low molecular weight compounds and in the liver toxicity.^{6–8} Furthermore, there is evidence that

shows that CYP2E1 is also associated with alcohol consumption,⁶ diabetes,⁹ and obesity¹⁰ as well as fasting.¹¹ There is thus also tremendous interest in this enzyme in terms of its influence on human health.

The active site for the majority of the monoxidation reactions that cytochrome P450 enzymes catalyze contains a heme group, which can form a ferryl-porphyrin- π cation radical, also called “Compound I” (CpdI) during the catalytic processes.¹² Some cytochrome P450 enzymes, such as CYP2A1, CYP2E1, CYP2B1, and CYP3A4, show atypical steady-state kinetics *in vitro* and presumably *in vivo*. In particular, for these enzymes, the reaction proceeds by the cooperative binding of two substrates simultaneously to form a ternary complex. The substrate that binds in the active site is usually called active substrate, while the other one that binds in the effector site, and that controls the oxidation

Received: August 28, 2011

Published: November 12, 2011

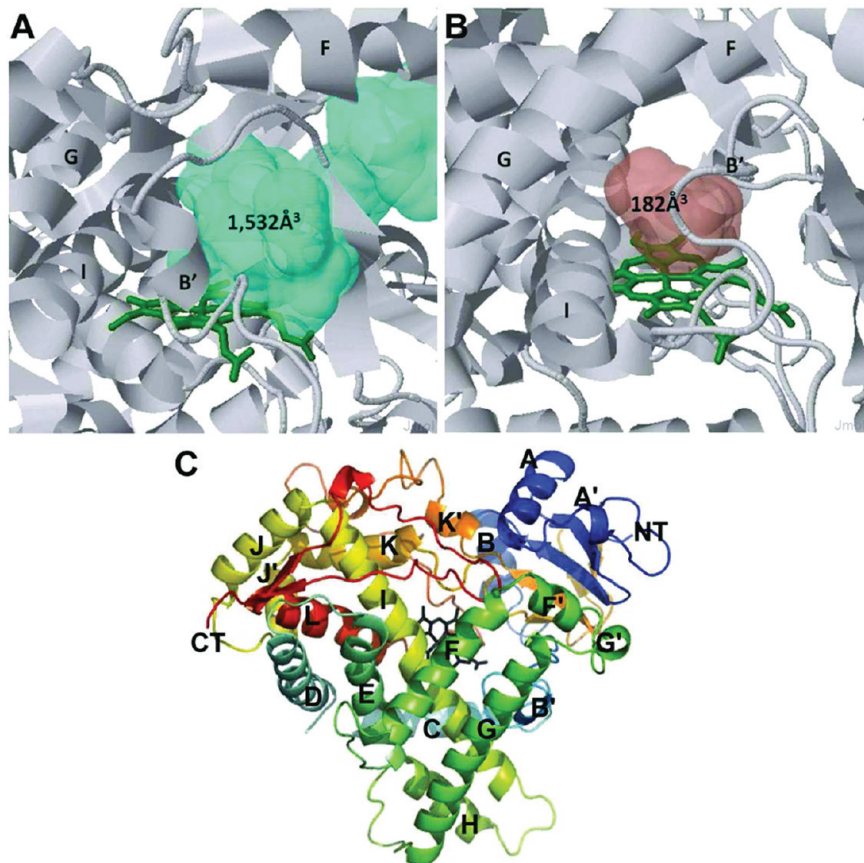


Figure 1. Ribbon diagram of the active site cavity and entire structure of human CYP2E1. (A) active site volume of human CYP3A4 (Protein Data Bank code 1tqn), (B) active site volume of human CYP2E1 (Protein Data Bank code 3e4e). The volumes were calculated by online tool Q-SiteFinder. (C) Distal face of the overall structure of human CYP2E1 rainbow colored from N-terminal (blue) to C-terminal (red). NT and CT denote the N- and C-terminal.

of the active substrate is called effector substrate. Some of these enzymes exhibit positive cooperativity and some negative cooperativity. CYP3A4 is a prototypical case of this family that exhibits positive cooperativity.¹³ Although the precise mechanism of the cooperative binding still remains unknown, it is believed to be related to the ability of the CYP3A4 enzyme to accommodate multiple substrates within its active site.^{14–16} Owing to the large size of this active site (Figure 1A), the effector substrate within CYP3A4 can have a direct effect on the active one, stabilizing the active substrate in the active site and enhancing a favorable orientation of the active substrate for oxidation.¹⁷ CYP2E1 however exhibits negative cooperativity.¹⁸ Koop reported the first example of the negative cooperativity for the monocyclic substrate pNP oxidation. At a low concentration, pNP was rapidly turned over (47 min^{-1}) with a low K_m value ($24 \mu\text{M}$); whereas at a high concentration ($>100 \mu\text{M}$), the oxidation rate of pNP gradually decreased as a second substrate bound to the enzyme at an effector site ($K_{ss} = 260 \mu\text{M}$).¹⁹ Since then, many good attempts have been made to conform the novel substrate inhibition mechanism.^{20,21} Compared to CYP3A4, the active site of CYP2E1 is much smaller ($182 \text{ cubic } \text{\AA}$ for CYP2E1 compared with $\sim 1532 \text{ cubic } \text{\AA}$ for CYP3A4, Figure 1B), and so the effector substrate cannot possibly bind within the active site. Thus, it is believed that the negative cooperativity observed in CYP2E1 occurs by a completely different mechanism. A deeper mechanistic understanding of the negative cooperativity

in human CYP2E1 should improve the predictions for drug–drug interactions and drug metabolism, which is a fundamental area of both mechanistic and pharmaceutical import.

Thus, to this end, we performed all-atom molecular dynamics simulations and free energy calculations to study the negative cooperative binding models of human CYP2E1. As the active and effector sites of human CYP2E1 are very narrow, we have to select the substrates as small as possible. So, in this study we only focus on the monocyclic substrates, which are believed to be the smallest substrates for human CYP2E1. Another reason for selecting monocyclic substrates is that only these substrates have been reported to undergo cooperativity in human CYP2E1.^{18–21} Thus, we focused our studies on the small monocyclic substrate of human CYP2E1, aniline, as the active and effector substrate. We first docked an aniline molecule into the active site of human CYP2E1 to form a set of single-ligand binding models. Subsequently we docked the second aniline into the effector site of human CYP2E1 near L103, L210, and F478 to form cooperative binding models. Finally, we employed molecular dynamics simulations and free energy calculations to investigate the single-ligand and cooperative binding models. Based on the molecular dynamics trajectories and covariance analysis, we found that the effector substrate can directly interacted with active site residues, thereby weakening the interactions of the active substrate with the active site of human CYP2E1.

METHODS AND COMPUTATIONAL DETAILS

Starting Structures. At the moment, there are in total five three-dimensional structures of human CYP2E1 in the Protein Data Bank, three with fatty acid substrates²² and two with low molecular weight substrates.²³ The initial protein structure in our study is thus obtained from 3e4e.pdb for its comparatively higher resolution and low molecular weight substrates.²³ It is a crystal structure of human CYP2E1 in complex with the inhibitor 4-methylpyrazole released in 2008 with a resolution of 2.20 Å. The missing residues (M138, G139, and K140) in this crystal structure were added using the Swiss-Pdb Viewer. Except for the polar hydrogen and heavy atoms of human CYP2E1 and CpdI, all others atoms including nonpolar hydrogens in this crystal structure were removed. The pK_a values for each residue in the CYP2E1 structure were calculated by using Delphi^{24,25} as a Poisson–Boltzmann solver with a dielectric constant of 4. Hydrogen atoms were subsequently added to the CYP2E1 structure with the t-Leap procedure of AMBER 9.0²⁶ based on the computational pK_a values mentioned above, to give a total charge of +1. Subsequently, CYP2E1 together with anilines and the heme group was solvated in a simulation box with ~18 694 explicit TIP3P water molecules. To neutralize the system, a chloride ion was added to random place a water molecule in the simulation box. The atoms of CYP2E1 and anilines were parametrized by Amber force field parameters.²⁷ The force field parameters of CpdI were obtained from previous QM/MM simulations.²⁸

Docking Procedure. As the active and effector sites for human CYP2E1 are small, only some small substrates can simultaneously bind in the active and effector sites. In this study, we only focus on the monocyclic substrates, since cooperativity in human CYP2E1 detected by biochemical studies is associated with these substrates.¹⁸ Aniline, the smallest monocyclic substrate of human CYP2E1 was thus selected as the active and effector substrates. We randomly selected 10 configurations in the molecular dynamics trajectory of the substrate-free system, then docked one aniline into the active site of these configurations using AutoDock 4.0.^{29–31} The genetic algorithm was used to perform 1000 independent runs for each configurations mentioned above on a 60 Å cubic grid, centered on the mass center of the aniline with a grid spacing of 0.375 Å. For each configuration, the binding model with comparatively low binding energy and the active aniline in a favorable orientation for hydroxylation were selected as the active binding models for the further docking and molecular dynamics simulations. Based on the previous works involving crystal structure analyses, site-direct mutagenesis, and theoretical studies,^{20,32} we identified the effector site of CYP2E1 as within the region near L103, L210, and F478. Thus, we docked the second aniline into the effector site of the aforementioned active binding models to obtain 10 cooperative binding models. Both active binding and cooperative binding models were then subjected to short molecular dynamics simulations to optimize the atomic coordinates, and the last frame of these simulations was finally used as the starting structures for the further molecular dynamics simulations. The active/effector site volumes were then calculated using online tool Q-SiteFinder.³³

Molecular Dynamics Simulations. There are totally three all-atoms models involved in our study and denoted as the substrate-free system (no ligand in either active or effector sites), the single-ligand binding system (one aniline bound in the active site), and the cooperative binding system (two aniline molecules bound in both active and effector sites), respectively. For each

simulated system, 10 independent simulations were carried out using the models obtained from previous docking procedures as starting structures. After solvation, all the models were subjected to steepest descent energy minimization (~2000 steps), followed by conjugate gradient for the next 1500 steps, and subsequently equilibrated with CYP2E1, CpdI, and aniline atoms fixed by 1 ns (ns) molecular dynamics to reduce the van der Waals conflicts. Finally, 10 ns molecular dynamics simulations were performed under the normal temperature (310 K) by AMBER 9.0 package with periodic boundary conditions in NPT ensemble. The SHAKE algorithm with a tolerance of 10⁻⁶ was applied to constrain all bonds in the systems involving hydrogen atoms, and atoms velocities for start-up runs were obtained according to the Maxwell distribution at 310 K. The isothermal compressibility was set to 4.5 × 10⁻⁵ bar for solvent simulations. The electrostatic interactions were treated by particle mesh Ewald (PME) algorithm with interpolation order of 4 and a grid spacing of 0.12 nm. The van der Waals interactions were calculated by using a cutoff of 12 Å. All the molecular dynamics simulations were performed with a time step of 1 fs (fs), and coordinates for all the models were saved every 1 ps (ps).

Free Energy Calculations. The molecular mechanics Poisson–Boltzmann surface area (MM-PB/SA) and molecular mechanics generalized Born surface area (MM-GB/SA) methods implemented in Amber 9.0 was applied to calculate the binding free energy for the active substrate. The principles of the MM-PB/SA and MM-GB/SA methods can be summarized as

$$\Delta G_{\text{bind}} = G_{\text{complex}} - (G_{\text{protein}} + G_{\text{ligand}}) \quad (1)$$

$$G \cong E_{\text{gas}} - TS_{\text{config}} + G_{\text{sol}} \quad (2)$$

$$E_{\text{gas}} = E_{\text{bond}} + E_{\text{angle}} + E_{\text{torsion}} + E_{\text{vdW}} + E_{\text{ele}} \quad (3)$$

$$G_{\text{sol}} = G_{\text{ele}} + G_{\text{nonpolar}} \quad (4)$$

In eq 1, the binding free energy change (ΔG) is calculated as the difference between the free energies of the complex (G_{complex}) and the protein (G_{protein}) as well as the ligand (G_{ligand}). These free energies are computed through eq 2 by summing up its internal energy in the gas phase (E_{gas}), the solvation free energy (G_{sol}), and a vibrational entropy term (TS). As the systems involved in our study have similar entropy, the entropy contributions are neglected with an aim of comparisons of the free energy differences for the active substrate between single-ligand binding and cooperative binding systems. E_{gas} is a standard force field energy calculated from eq 3 by the strain energies from covalent bonds (E_{bond} and E_{angle}) and torsion angles (E_{torsion}), noncovalent van der Waals (E_{vdW}), and electrostatic energies (E_{ele}). As described in eq 4, the solvation free energy (G_{sol}) is computed by both an electrostatic term (G_{ele}) and a nonpolar component (G_{nonpolar}). The former can be obtained from either the Poission–Boltzman method (PB) or the generalized Born (GB) method. The latter is considered to be proportional to the molecular solvent accessible surface area (SASA). In our study, a total 200 snapshots retrieved from the last 1 ns segment on the simulation trajectories with an interval of 5 ps were used for the binding free energy calculations.

Covariance Analysis. In order to study the significant motions in the single-ligand binding and cooperative binding systems, covariance matrix plots for all the Cα atoms were calculated from the last 5 ns molecular dynamics simulations.

The covariance used in our study is defined as following:

$$S_{i,j} = \frac{\langle x_i x_j \rangle}{[\langle x_i^2 \rangle \langle x_j^2 \rangle]^{1/2}} \quad (5)$$

In eq 5, x_i and x_j are the coordinate displacements relative to the average positions of atoms i and j . By diagonalizing the covariance matrix, the anharmonic and large-scale motions of the protein are isolated from the harmonic and short-scale motions by reason that the anharmonic and large-scale motions in proteins or enzymes are often correlated to its biological functions. Similar approach has been widely used to analyze the molecular dynamics simulation trajectories in recent research papers.^{34–39} In this study, the covariance matrix is used to inspect correlated alterations in terms of side chain movements within the active site upon addition of the effector substrate.

RESULTS AND DISCUSSION

Trajectory Analysis. As the root-mean-square (rms) deviation from the starting structure is considered as a central criterion to measure the convergence of the simulated systems, we first calculated the rms deviation values for all the $C\alpha$ atoms (Figure 2A). As the enzymes in cytochrome P450 family share a conserved folding structure with negligible variation, no significant rms deviation fluctuations were expected to occur. Thus the rms deviation values for all the simulated systems did not change significantly from their starting structures. The final rms deviation values for all the simulated systems were no more than 2 Å, indicating that all the simulated systems were equilibrated. This observation also showed that the substrate binding did not lead to notable structural alterations for the entire protein, which agrees with the theoretical study of human CYP3A4 in their report on the positive cooperativity of cytochrome enzymes. We also studied the case of a single substrate in the effector site using molecular dynamics simulations. However, in this case, the protein was not stable as the aforementioned systems. The rms deviation values for the $C\alpha$ atoms were over 2 Å (Supporting Information, Figure S1), much larger than the other simulated systems. This observation was mainly caused by the substrate movement. The substrate binding in the effector site was not stable, as after several picoseconds it diffused away from the effector site via a substrate access channel (Supporting Information, Figure S2), suggesting that the effector site is not the first binding site of human CYP2E1.

To detect the structural fluctuations in human CYP2E1, we further computed the rms fluctuation values for each residue (Figure 2B). During our simulations, significant structural fluctuations were detected in the residues located in B' helix, F helix, I helix, and the loop between K helix and β 1–4 as well as β 4–1/ β 4–2 turn (Figure 1C). These residues together with CpdI constitute an active site cavity or pocket for the low molecular weight substrates of human CYP2E1. Agreeing with the crystal studies, our calculations showed that the size of this active site is only 190 cubic Å, which is the smallest observed active site volume for human cytochrome enzymes and probably the reason for the preference of human CYP2E1 for low molecular weight substrates. By directly interacting with the active substrates, residues in the active site are believed to play an important role to recognize the substrates and to position them in the right direction for further metabolism reactions.

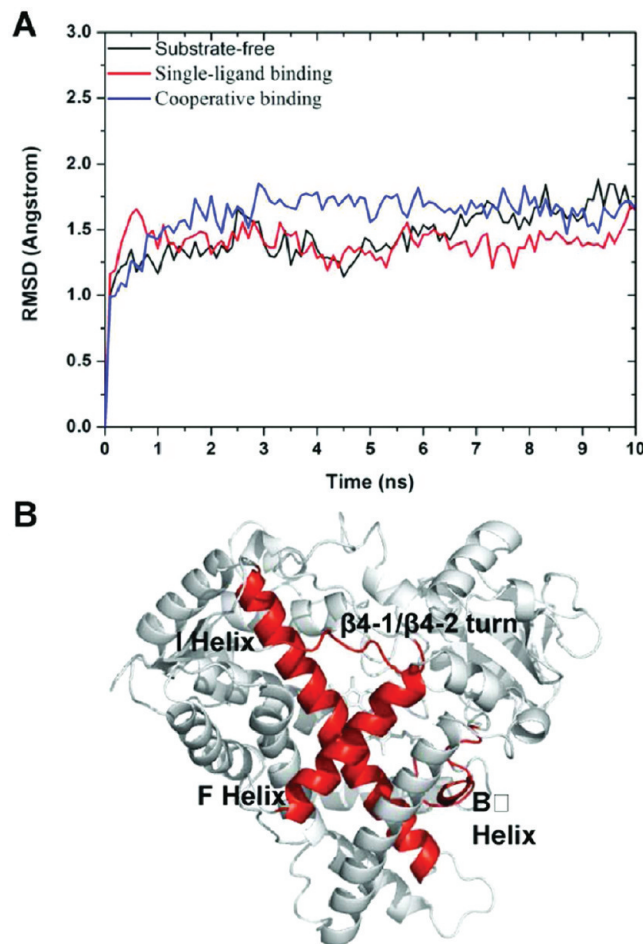


Figure 2. Rms deviation and fluctuation of all the $C\alpha$ atoms. (A) Time-dependent rms deviation values from the starting structures along the simulation trajectories for substrate-free, single-ligand binding, and cooperative binding systems, respectively. (B) Illustratively showing the highlight regions with significant rms fluctuations (colored in red) on the overall structure of human CYP2E1.

Close Contact analysis. To characterize the interactions between active site residues and substrates, the close contacts defined as the ones less than 5 Å between substrates and the protein were calculated along the molecular dynamics simulation trajectories for all the simulated systems (Figure 3). As expected, the residues employing close contacts with the active substrates were mainly located in the active site. These residues (I115 in B' helix; F207 in F helix; F298, A299, G302, and T303 in I helix; L363, V364, and L368 in the loop between K helix and β 1–4; F478 in β 4–1/ β 4–2 turn) have significant close contacts with the active substrate in more than 80% frames in the simulation trajectories for both single-ligand binding and cooperative binding systems. Additional analyses showed that these residues were able to stabilize the active substrate by nonbonding interactions. T303 in I helix was found to form a significant hydrogen bond with the active substrate, which could fix the active substrate in a favorable position for the further metabolic reaction. As located in the same helix near T303, F298, A299, and G302 had abilities to influence the aforementioned hydrogen-bonding interaction formed by residue interactions. The residues I115, F207, L363, V364, and L368 were mainly located in the active site, providing hydrophobic interactions to stabilize the active substrate.

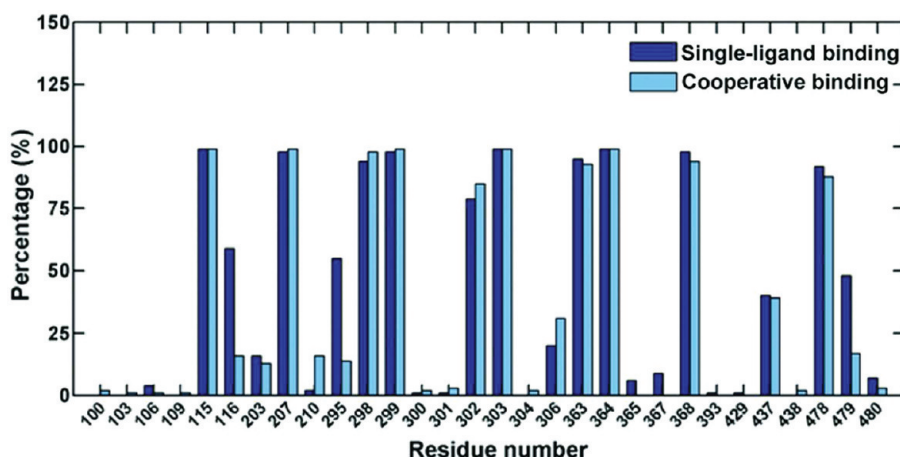


Figure 3. Percentage of frames over the simulation trajectories that have close contacts of less than 5 Å between the active substrate and the residues for the single-ligand binding and cooperative binding systems.

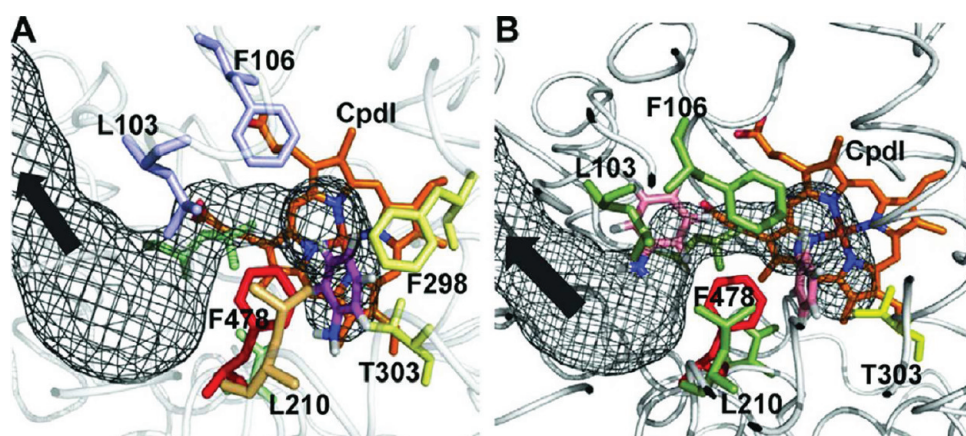


Figure 4. Stereo view of the key residues in the active site of human CYP2E1 for (A) single-ligand binding and (B) cooperative binding systems, respectively. The substrate access is shown in black mesh. The residues and Cpdl are shown in stick representations.

This point is further supported by the fact that V364L, L368 V, and F478 V in human CYP2E1 are able to lower the substrate hydroxylation activity relevant to the wild-type protein.³² F478 in $\beta 4-1/\beta 4-2$ turn was shared by the active and effector sites, indicating that this residue can interact with both substrates. As the substrate involved in our study was a monocyclic compound, this residue was found to have $\pi-\pi$ stacking interactions. Thus based on these observations, we believed that these residues in the active site were important for human CYP2E1 specificity and might play crucial roles in positioning the active substrates by recontouring the active site volume.

Additionally, significant variations of the close contacts between the single-ligand binding and cooperative binding systems were mainly detected in residues F116, L210, D295, and G479. In the single-ligand binding system, ~60% frames in the simulated trajectories had close contacts of F116, D295, and G479 with the active substrates. However no more than 25% of frames in the cooperative binding system exhibited such interactions. One reasonable explanation for this observation is that the effector substrate binding stabilizes these residues further away from the active substrate, so as to weaken the interactions of the active substrate with the active site residues, leading to the abasement of the metabolic efficiency.

Different from the aforementioned residues, no close contact was detected in the single-ligand binding systems for L210, which however exhibited significant close contacts with almost 25% frames in the cooperative binding system. This observation is consistent with previous homology modeling studies of human CYP2E1. As this residue is not a component of the active site cavity, it is not expected that the active substrate can directly interact with this residue. However, according to the mutagenesis analysis, L210I mutation can lead to less substrate hydroxylation activity.^{23,32} Based on our simulations and crystal structure analysis, it is believed that L210 is capable of packing against the aromatic ring of F478 between the substrate access channel and the active site cavity (Figure 4). Thus altering the amino acid at this position can have an indirect effect on substrate access or on ligand positioning in the active site.

Covariance Analysis. In order to study the significant motions in the single-ligand binding and cooperative binding system, covariance matrix plots for all the $C\alpha$ atoms were calculated from the last 5 ns molecular dynamics simulations. The covariance matrix used in our study was defined by eq 5. By diagonalizing the covariance matrix, the anharmonic and large-scale motions of the protein are isolated from the harmonic and short-scale motions by reason that the anharmonic and large-scale motions in proteins or

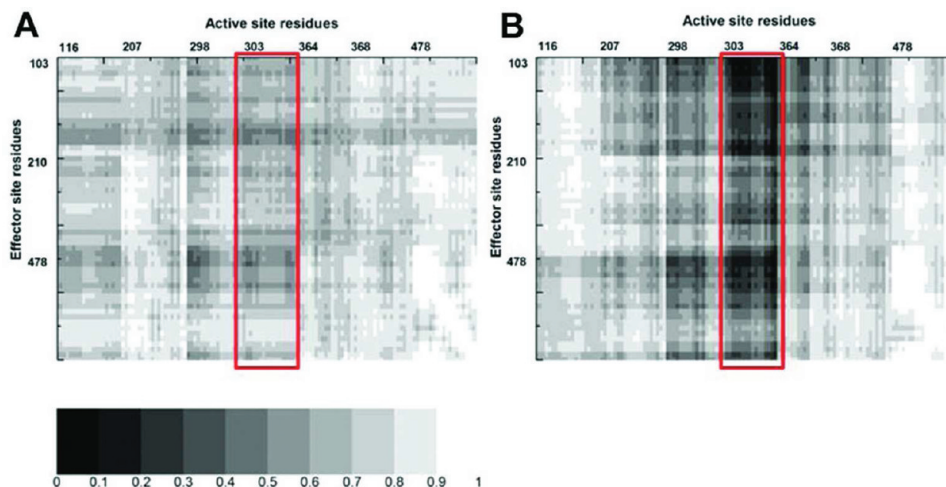


Figure 5. Covariance matrix plots of the spatial displacement between the atoms of the key residues in the active and effector sites for (A) single-ligand binding and (B) cooperatively binding systems, respectively.

enzymes are often correlated to its biological functions. In our study, the covariance matrix is used to inspect correlated alterations in terms of side chain movements within the active site upon addition of the effector substrate.

To obtain molecular insight into the spatial cross talk between the core residues in the active and effector sites, the covariance matrix plots calculated between the key residues in the active site and in the effector site were shown in Figure 5. In the single-ligand binding system, the selected residues in both active and effector sites employed strong positive correlations according to their covariance values. The correlation between the active and effector sites is mainly associated with F478, the residue shared by the active and effector sites, and regarded as a linker between the active and effector sites. However, the correlations sharply decreased in the cooperative binding system. Notably, the correlation of T303 with the effector site residues almost disappeared in the cooperative binding system. According to the mutagenesis studies,^{40–42} this residue is a key factor in the substrate positioning. This is further confirmed by the crystal studies of human CYP2E1,²³ in which T303 forms a significant hydrogen bond with the substrate. Of most importance, some evidence also suggests that this conserved residue plays a crucial role in proton delivery to the active site in CYP2E1 and other cytochrome enzymes.^{43–46} In our simulations, this conserved residue could form an important hydrogen bond with the active aniline, which was believed to keep the active substrate in a favorable position for the further metabolic reaction. Upon the effector substrate binding, the significant interactions for the residues in the active and effector sites were changed, making T303 to adopt a different side-chain configuration which was not able to form hydrogen-bonding interactions with the active substrate. Thus, the disappearance of the positive correlation for T303 with the effector site residues may not keep the active substrate in the correct position and may destroy the proton delivery to the active site in human CYP2E1, further reducing the metabolic efficiency of the active substrates. Interestingly, in the case of a single-ligand binding in the effector site, the correlation of T303 was found to recover after 1.3 ps molecular dynamics simulations (Supporting Information, Figure S3).

Free Energy Calculation. To get greater insight into the active substrate interactions with the enzyme, we performed free

Table 1. Binding Free Energies (kcal/mol) Calculated by the MM-PB/SA and MM-GB/SA Methods for the Active Substrate in Both Single-Ligand Binding and Cooperative Binding Systems^a

energies (kcal/mol)	single-ligand binding	cooperative binding
ΔE_{ele}	-3.44 ± 2.31	-2.45 ± 2.02
ΔE_{vdW}	-14.15 ± 1.88	-13.50 ± 1.33
ΔE_{gas}	-17.60 ± 3.71	-15.95 ± 2.95
$\Delta G_{\text{nonpolar/PB}}$	-1.74 ± 0.08	-1.83 ± 0.15
$\Delta G_{\text{ele/PB}}$	11.95 ± 2.72	12.02 ± 2.51
$\Delta G_{\text{sol/PB}}$	10.21 ± 2.71	10.18 ± 2.50
$\Delta G_{\text{bind/PB}}$	-7.39 ± 3.52	-5.77 ± 3.67
$\Delta G_{\text{nonpolar/GB}}$	-2.51 ± 0.12	-2.64 ± 0.21
$\Delta G_{\text{ele/GB}}$	10.34 ± 2.09	9.19 ± 1.90
$\Delta G_{\text{sol/GB}}$	7.83 ± 2.12	6.55 ± 1.97
$\Delta G_{\text{bind/GB}}$	-9.77 ± 2.09	-9.40 ± 1.55

^a $\Delta E_{\text{gas}} = \Delta E_{\text{ele}} + \Delta E_{\text{vdW}}$; $\Delta G_{\text{sol/PB}} = \Delta G_{\text{ele/PB}} + \Delta G_{\text{non-polar/PB}}$; $\Delta G_{\text{bind/PB}} = \Delta E_{\text{gas}} + \Delta G_{\text{sol/PB}} - T\Delta S$; $\Delta G_{\text{bind/GB}} = \Delta E_{\text{gas}} + \Delta G_{\text{sol/GB}} - T\Delta S$.

energy calculations for the active substrate using both MM-PB/SA and MM-GB/SA methods. The binding free energies for the active substrate in the single-ligand binding system were -7.39 ± 3.52 kcal/mol (by MM-PB/SA) and -9.77 ± 2.09 kcal/mol (by MM-GB/SA), while those for the cooperative binding system were -5.77 ± 3.67 kcal/mol (by MM-PB/SA) and -9.40 ± 1.55 kcal/mol (by MM-GB/SA), respectively (Table 1). It was found that using MM-PB/SA approach the binding free energy for the active substrate is much smaller in the cooperative binding system. However, using MM-GB/SA approach, the difference of the binding free energy for both systems was only ~ 0.3 kcal/mol. This variation is mainly caused by the different methods (Poisson-Boltzman approach in MM-PB/SA and Generalized Born approach in MM-GB/SA) for calculating the electrostatic term in the solvation free energy. However, due to the comparatively large standard deviations of the binding free energies, the differences between the single-ligand binding and cooperative binding systems were thought to be not significant, indicating that the effector substrate employed few

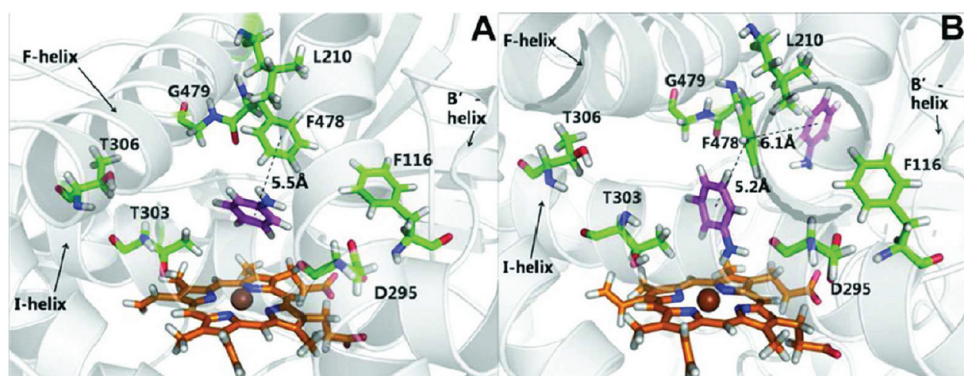


Figure 6. Illustratively showing the $\pi-\pi$ stacking interactions between the active/effect substrate and residue F478 for (A) single-ligand binding and (B) cooperative binding systems, respectively. All the molecules are shown in stick representations. The hydrogen, nitrogen, and oxygen atoms are colored in white, blue, and red, respectively. The carbon atoms for HEME, active/effect substrate, and residue F478 are colored in brown, pink, and green, respectively.

influence on the binding affinity of the active substrate. As mentioned in the previous discussions, a single substrate binding in the effector site alone is not stable. However, after the active substrate binding in the active site, the effector substrate can be stable in the effector site, indicating that the active site should be the primary binding site of substrates and that the presence of the active substrate is able to stabilize the second substrate in the effector site in human CYP2E1.

Based on the energy term analysis, the variations of the binding free energies for the single-ligand binding and cooperative binding systems are mainly focused on the electrostatic energies (ΔE_{ele}) and noncovalent van der Waals (ΔE_{vdw}). The former for the single-ligand binding and cooperative binding systems are -3.44 ± 2.31 kcal/mol (by MM-PB/SA) and -2.45 ± 2.02 kcal/mol (by MM-GB/SA), respectively (Table 1). By carefully looking into the simulation trajectories, we found that this variation was mainly caused by the $\pi-\pi$ stacking interactions between the active substrate, residue F478, and the effector substrate. As defined by previous theoretical studies,^{47,48} if the distance between the mass centers of the aromatic rings for two molecules is less than 7 Å, then it is believed that there are $\pi-\pi$ stacking interactions between these two molecules. Thus, we calculated the distances of the mass center between the aromatic rings of the active substrate, F478, and the effector substrate (Figure 6A). The average distances between the active substrate and residue F478 are 5.50 ± 0.85 and 5.20 ± 0.64 Å for the single-ligand binding and cooperative binding systems, respectively, while that for the effector substrate and residue F478 is 6.10 ± 0.95 Å. Based on the aforementioned definition, it is concluded that both active and effector substrates employ $\pi-\pi$ stacking interactions with residue F478 in most of configurations (~80% frames) along the simulation trajectories. Additionally, we also calculated the angles between the aromatic rings of both active and effector substrates with residue F478 and found that the active substrate in the single-ligand binding system is disposed to be the configuration parallel to the aromatic ring of residue F478 (about 70–90°, see Figure 6B). In such configuration, the hydroxylation site of the active substrate is close to CpdI, leading to the hydroxylation reaction occurring easily. However, after the effector substrate binding in the cooperative binding system, the active substrate is inclined to have an angle of 40–60° with the aromatic ring of residue F478 (Figure 6C), making the hydroxylation site of the active substrate a little far away from CpdI.

In addition to the binding free energies for the active substrate, we also computed the residue contributions to the binding free energies (Supporting Information, Table S1). As expected, the residues in the active site cavity (I115 and F116 in B' helix; F207 and L210 in F helix; D295, F298, A299, G302, and T303 in I helix; L363, V364, and L368 in the loop between K helix and $\beta 1-4$; and F478 in $\beta 4-1/\beta 4-2$ turn) have significant contributions to the binding free energies of the active substrate, which agrees with the previous discussions on rms deviation and fluctuations as well as the close contact analysis. However, the residue contributions to the binding free energy for the active site residues in the cooperative binding system were much higher than those in the single-ligand binding system. For example, the energy contributions for I115 and F116 in B' helix in the single-ligand binding system were about -0.50 ± 0.20 and 0.00 ± 0.03 kcal/mol, while those in the cooperative binding system increased to 0.12 ± 0.27 and 1.22 ± 0.36 kcal/mol, respectively. This change was mainly caused by the reorientation of the side chain. The energy contributions of the backbone atoms for I115 and F116 in both single-ligand binding and cooperative binding systems were almost the same, but those of the side chain atoms changed significantly. The energy contributions of the side chain atoms for the two residues in the single-ligand binding system were -0.47 ± 0.19 and -0.01 ± 0.03 kcal/mol, while those in the cooperative binding system were 0.07 ± 0.24 and 1.18 ± 0.34 kcal/mol, respectively. In contrast, the energy contributions for some residues (G302 and T303 in I helix, and L363 in the loop between K helix and $\beta 1-4$) in the cooperative binding system were comparatively lower than those in the single-ligand binding system. These residues were mainly located on I helix and the loop between K helix and $\beta 1-4$, near the active substrate but a little further away from the CpdI. The lower energy contributions in the cooperative binding system showed that the active substrate in this case would be preferred to bind near these residues, further away from the catalytic center of human CYP2E1, which would reduce its metabolic efficiency.

CONCLUSION

In order to gain molecular insights into the mechanism of the negative cooperative binding in human CYP2E1, we employed molecular dynamics simulations to study the impact of the addition of an effector substrate on an active substrate in

the active site of human CYP2E1 and on the interactions of this effector substrate with the protein. Our simulations indicate that the cooperative binding mechanism involves the interactions between the active substrate and the active site residues as well as between the effector substrate and the protein, thereby influencing the structural motions of side chains. Our findings suggest that the conserved T303 in I helix proximal to CpdI plays a crucial role in the negative cooperative binding on the short-range effects. This residue is a key factor in the positioning of substrates and in proton delivery to the active site, and the negative cooperative binding can reduce the activity of this residue. A long-range effect of the effector substrate is identified in which F478 is proposed to play an important role. F478 is considered as a structural linker of the active and effector sites, locating between the substrate access channel and the active site and exhibiting direct effects on substrate access or on ligand positioning in the active site. In the negative cooperative binding, this residue can decrease the interactions of the active substrates with the active site by $\pi-\pi$ stacking so as to lower the hydroxylation activity for the active substrate. These findings can give atomic insights into the negative cooperative binding of human CYP2E1, providing useful information for drug metabolism and personalized drug design.

ASSOCIATED CONTENT

Supporting Information. Results from free energy calculations, the rms deviation values for the case of a single substrate binding in the effector site alone, and some additional figures. This information is available free of charge via the Internet at <http://pubs.acs.org>.

AUTHOR INFORMATION

Corresponding Author

*E-mail: dqwei@sjtu.edu.cn; jfwang8113@sjtu.edu.cn.

ACKNOWLEDGMENT

This work was supported by the grants from National Basic Research Program of China (973 Program, 2011CB910204 and 2012CB721000), National Natural Science Foundation of China (nos. 30870476, 30900272, and 90913009), Shanghai Natural Science Foundation (no.10ZR1421500), China Postdoctoral Science Foundation (no.20110490068), and Chinese Academy of Sciences (KSCX2-YW-R-112).

REFERENCES

- Danielson, P. B. The Cytochrome P450 superfamily: biochemistry, evolution and drug metabolism in humans. *Curr. Drug Metab.* **2002**, *3*, 561–597.
- Wang, J. F.; Zhang, C. C.; Chou, K. C.; Wei, D. Q. Structure of cytochrome P450s and personalized drug. *Curr. Med. Chem.* **2009**, *16*, 232–244.
- Guengerich, F. P. Catalytic selectivity of human cytochrome P450 enzymes: relevance to drug metabolism and toxicity. *Toxicol. Lett.* **1994**, *70*, 133–138.
- Wang, J. F.; Chou, K. C. Molecular modeling of cytochrome P450 and drug metabolism. *Curr. Drug Metab.* **2010**, *11*, 342–346.
- Chen, Q.; Zhang, T.; Wang, J. F.; Wei, D. Q. Advances in human cytochrome P450 and personalized medicine. *Curr. Drug Metab.* **2011**, *12*, 436–444.
- Ioannides, C.; Lewis, D. F. Cytochromes P450 in the bioactivation of chemicals. *Curr. Top. Med. Chem.* **2004**, *4*, 1767–1788.
- Nanji, A. A.; Zhao, S.; Sadrzadeh, S. M.; Dannenberg, A. J.; Tahan, S. R.; Waxman, D. J. Markedly enhanced cytochrome P450 2E1 induction and lipid peroxidation is associated with severe liver injury in fish oil-ethanol-fed rats. *Alcohol.: Clin. Exp. Res.* **1994**, *18*, 1280–1285.
- Trafalis, D. T.; Panteli, E. S.; Grivas, A.; Tsigris, C.; Karamanakos, P. N. CYP2E1 and risk of chemically mediated cancers. *Expert. Opin. Drug Metab. Toxicol.* **2010**, *6*, 307–319.
- Barnett, C. R.; Rudd, S.; Flatt, P. R.; Ioannides, C. Sex differences in the diabetes-induced modulation of rat hepatic cytochrome P450 proteins. *Biochem. Pharmacol.* **1993**, *45*, 313–319.
- Raucy, J. L.; Lasker, J. M.; Kraner, J. C.; Salazar, D. E.; Lieber, C. S.; Corcoran, G. B. Induction of cytochrome P450IIIE1 in the obese overfed rat. *Mol. Pharmacol.* **1991**, *39*, 275–280.
- Johansson, I.; Ekstrom, G.; Scholte, B.; Puzycki, D.; Jornvall, H.; Ingelman-Sundberg, M. Ethanol-, fasting-, and acetone-inducible cytochromes P-450 in rat liver: regulation and characteristics of enzymes belonging to the IIB and IIE gene subfamilies. *Biochemistry* **1988**, *27*, 1925–1934.
- Meunier, B.; de Visser, S. P.; Shaik, S. Mechanism of oxidation reactions catalyzed by cytochrome P450 enzymes. *Chem. Rev.* **2004**, *104*, 3947–3980.
- Domanski, T. L.; Liu, J.; Harlow, G. R.; Halpert, J. R. *Arch. Biochem. Biophys.* **1998**, *350*, 223–232.
- Shou, M.; Grogan, J.; Mancewicz, J. A.; Krausz, K. W.; Gonzalez, F. J.; Belboin, H. V.; Korzekwa, K. R. Activation of CYP3A4: evidence for the simultaneous binding of two substrates in a cytochrome P450 active site. *Biochemistry* **1994**, *33*, 6450–6455.
- Korzekwa, K. R.; Krishnamachary, N.; Shou, M.; Ogai, A.; Parise, R. A.; Rettie, A. E.; Gonzalez, F. J.; Tracy, T. S. Evaluation of atypical cytochrome P450 kinetics with two-substrate models: evidence that multiple substrates can simultaneously bind to cytochrome P450 active site. *Biochemistry* **1998**, *37*, 4137–4147.
- He, Y. A.; Roussel, F.; Halpert, J. R. Analysis of homotropic and heterotropic cooperativity of diazepam oxidation by CYP3A4 using site-directed mutagenesis and kinetic modeling. *Arch. Biochem. Biophys.* **2003**, *409*, 92–101.
- Fishelovitch, D.; Hazan, C.; Shaik, S.; Wolfson, H. J.; Nussinov, R. Structural dynamics of the cooperative binding of organic molecules in the human cytochrome P450 3A4. *J. Am. Chem. Soc.* **2007**, *129*, 1602–1611.
- Miller, G. P. Advances in the interpretation and prediction of CYP2E1 metabolism from a biochemical perspective. *Expert. Opin. Drug Metab. Toxicol.* **2008**, *4*, 1053–1064.
- Koop, D. R. Hydroxylation of p-nitrophenol by rabbit ethanol-inducible cytochrome P450 isozyme 3a. *Mol. Pharmacol.* **1986**, *29*, 399–404.
- Collom, S. L.; Laddusaw, R. M.; Burch, A. M.; Kuzmic, P.; Perry, M. D.; Miller, G. P. CYP2E1 substrate inhibition: Mechanistic interpretation through an effector site for monocyclic compounds. *J. Biol. Chem.* **2008**, *283*, 3487–3496.
- Harrelson, J. P.; Atkins, W. M.; Nelson, S. D. Multiple-ligand binding in CYP2A6: probing mechanism of cytochrome P450 cooperativity by assessing substrate dynamics. *Biochemistry* **2008**, *47*, 2978–2988.
- Porubsky, P. R.; Battaile, K. P.; Scott, E. E. Human cytochrome P450 2E1 structures with fatty acid analogs reveal a previously unobserved binding mode. *J. Biol. Chem.* **2010**, *285*, 22282–22290.
- Porubsky, P. R.; Meneely, K. M.; Scott, E. E. Structures of human cytochrome P-450 2E1: Insights into the binding of inhibitors and both small molecular weight and fatty acid substrates. *J. Biol. Chem.* **2008**, *283*, 33698–33707.
- Georgescu, R. E.; Alexov, E. G.; Gunner, M. R. Combining conformational flexibility and continuum electrostatics for calculating pK(a)s in proteins. *Biophys. J.* **2002**, *83*, 1731–1748.
- Rocchia, W.; Alexov, E.; Honing, B. Extending the applicability of the nonlinear Poisson-Boltzmann equation: multiple dielectric constants and multivalent ions. *J. Phys. Chem. B* **2001**, *105*, 6507–6514.

- (26) Case, D. A.; Cheatham, T. E., 3rd; Darden, T.; Gohlke, H.; Luo, R.; Merz, K. M., Jr.; Onufriev, A.; Simmerling, C.; Wang, B.; Woods, R. J. The Amber biomolecular simulation program. *J. Comput. Chem.* **2005**, *26*, 1668–1688.
- (27) Ponder, J. W.; Case, D. A. Force field for protein simulations. *Adv. Protein Chem.* **2003**, *66*, 27–85.
- (28) Schoneboom, J. C.; Lin, H.; Reuter, N.; Thiel, W.; Cohen, S.; Ogliaro, F.; Shaik, S. The elusive oxidant species of cytochrome P450 enzymes: characterization by combined quantum mechanical/molecular mechanical (QM/MM) calculations. *J. Am. Chem. Soc.* **2002**, *124*, 8142–8151.
- (29) Goodsell, D. S.; Morris, G. M.; Olson, A. J. Automated docking of flexible ligands: applications of AutoDock. *J. Mol. Recognit.* **1996**, *9*, 1–5.
- (30) Morris, G. M.; Goodsell, D. S.; Halliday, R. S.; Huey, R.; Hart, W. E.; Belew, R. K.; Olson, A. J. Automated docking using a Lamarckian genetic algorithm and an empirical binding free energy function. *J. Comput. Chem.* **1998**, *19*, 1639–1662.
- (31) Huey, R.; Morris, G. M.; Olson, A. J.; Goodsell, D. S. A semiempirical free energy force field with charge-based desolvation. *J. Comput. Chem.* **2007**, *28*, 1145–1152.
- (32) Spatzenegger, M.; Liu, H.; Wang, Q.; Debarber, A.; Koop, D. R.; Halpert, J. R. Analysis of differential substrate selectivities of CYP2B6 and CYP2E1 by site-directed mutagenesis and molecular modeling. *J. Pharmacol. Exp. Ther.* **2003**, *304*, 477–487.
- (33) Laurie, A. T.; Jackson, R. M. Q-SiteFinder: an energy-based method for the prediction of protein-ligand binding sites. *Bioinformatics* **2005**, *21*, 1908–1916.
- (34) Lian, P.; Wei, D. Q.; Wang, J. F.; Chou, K. C. An allosteric mechanism inferred from molecular dynamics simulations on phospholamban pentamer in lipid membranes. *PLoS ONE* **2011**, *6*, e18587.
- (35) Wang, J. F.; Chou, K. C. Insights from modeling the 3D structure of New Delhi metabollo-beta-lactamase and its binding interactions with antibiotic drugs. *PLoS ONE* **2011**, *6*, e18414.
- (36) Wang, Y.; Wei, D. Q.; Wang, J. F. Molecular dynamics studies on T1 lipase: insight into a double-flap mechanism. *J. Chem. Inf. Model.* **2010**, *50*, 875–878.
- (37) Wang, J. F.; Chou, K. C. Insights from studying the mutation-induced allostery in the M2 proton channel by molecular dynamics. *Protein Eng., Des. Sel.* **2010**, *23*, 663–666.
- (38) Wang, J. F.; Chou, K. C. Insight into the molecular switch mechanism of human RabS_a from molecular dynamics simulations. *Biochem. Biophys. Res. Commun.* **2009**, *390*, 608–612.
- (39) Wang, J. F.; Wei, D. Q.; Chou, K. C. Insights from investigating the interactions of adamantane-based drugs with the M2 proton channel from the H1N1 swine virus. *Biochem. Biophys. Res. Commun.* **2009**, *388*, 413–417.
- (40) Fukuda, T.; Imai, Y.; Komori, M.; Kusunose, E.; Satouchi, K.; Kusunose, M. Replacement of Thr-303 of P450 2E1 with serine modifies the regioselectivity of its fatty acid hydroxylase activity. *J. Biochem.* **1993**, *113*, 7–12.
- (41) Fukuda, T.; Imai, Y.; Komori, M.; Nakamura, M.; Kusunose, E.; Satouchi, K.; Kusunose, M. Different mechanisms of regioselection of fatty acid hydroxylation by laurate (omega-1)-hydroxylating P450s, P450 2C2 and P450 2E1. *J. Biochem.* **1994**, *115*, 338–344.
- (42) Moreno, R.; Goosen, T.; Kent, U. M.; Chung, F. L.; Hollenberg, P. F. Differential effects of naturally occurring isothiocyanates on the activities of cytochrome P450 2E1 and the mutant P450 2E1 T303A. *Arch. Biochem. Biophys.* **2001**, *391*, 99–110.
- (43) Blobaum, A. L.; Kent, U. M.; Alworth, W. L.; Hollenberg, P. F. Novel reversible inactivation of cytochrome P450 2E1 T303A by tert-butylacelene: the role of threonine 303 in proton delivery to the active site of cytochrome P450 2E1. *J. Pharmacol. Exp. Ther.* **2004**, *310*, 281–290.
- (44) Imai, M.; Shimada, H.; Watanabe, Y.; Matsushima-Hibiya, Y.; Makino, R.; Koga, H.; Horiuchi, T.; Ishimura, Y. Uncoupling of the cytochrome P-450cam monooxygenase reaction by a single mutation, threonine-252 to alanine or valine: possible role of the hydroxyl amino acid in oxygen activation. *Proc. Natl. Acad. Sci. U.S.A.* **1989**, *86*, 7823–7827.
- (45) Vaz, A. D.; Pernecke, S. J.; Raner, G. M.; Coon, M. J. Peroxoiron oxenoid-iron species as alternative oxygenating agents in cytochrome P450-catalyzed reactions: switching by threonine-302 to alanine mutagenesis of cytochrome P450 2B4. *Proc. Natl. Acad. Sci. U.S.A.* **1996**, *93*, 4644–4648.
- (46) Vaz, A. D.; McGinnity, D. F.; Coon, M. J. Epoxidation of olefins by cytochrome P450: evidence from site-specific mutagenesis for hydroperoxy-iron as an electrophilic oxidant. *Proc. Natl. Acad. Sci. U.S.A.* **1998**, *95*, 3555–3560.
- (47) McGaughey, G. B.; Gagné, M.; Rappé, A. K. pi-Stacking interactions: Alive and well in proteins. *J. Biol. Chem.* **1998**, *273*, 15458–15463.
- (48) Burley, S. K.; Petsko, G. A. Aromatic-aromatic interaction: a mechanism of protein structure stabilization. *Science* **1985**, *229*, 23–28.